

Quantum Dot Light-Emitting Devices with Electroluminescence Tunable over the Entire Visible Spectrum

Polina O. Anikeeva,^{†,‡} Jonathan E. Halpert,^{†,§} Moungi G. Bawendi,[§] and Vladimir Bulović^{*,‡}

Laboratory of Organic Optics and Electronics, Department of Electrical Engineering and Computer Science, Massachusetts Institute of Technology, Cambridge Massachusetts 02139, and Department of Chemistry, Massachusetts Institute of Technology, Cambridge, Massachusetts 02139

Received January 28, 2009; Revised Manuscript Received May 1, 2009

ABSTRACT

Improvements in quantum dot light-emitting device (QD-LED) performance are achieved by the choice of organic charge transporting layers, by use of different colloidal QDs for the different parts of the visible spectrum, and by utilizing a recently demonstrated robust QD deposition method. Spectrally narrow electroluminescence of our QD-LEDs is tuned over the entire visible wavelength range from $\lambda = 460$ nm (blue) to $\lambda = 650$ nm (deep red). By printing close-packed monolayers of different QD types inside an identical QD-LED structure, we demonstrate that different color QD-LEDs with QDs of different chemistry can be fabricated on the same substrate. We discuss mechanisms responsible for efficiency increase for green (4-fold) and orange (30%) QD-LEDs as compared to previous reports and outline challenges associated with achieving high-efficiency blue QD-LEDs.

Hybrid organic–quantum dot light-emitting devices (QD-LEDs)^{1–10} combine the color purity and durability of QDs with the efficiency, flexibility, and low processing cost of organic light-emitting devices (OLEDs). Previous efforts to create efficient QD-LEDs demonstrated red, green, and blue (RGB) devices with external quantum efficiencies (EQEs) from 1.0% to 2.1%,^{6–10} from 0.5% to 0.65%,^{9–11} and from 0.2% to 0.3%,^{9,12} respectively. However, state-of-the-art OLEDs currently used in consumer electronics can be >10% quantum efficient.¹³ The high color quality (saturated emission and precisely tunable peak emission wavelength) distinguishes QD-LEDs over other technologies, but to be ultimately competitive in every performance category improvements in QD-LED quantum efficiencies as well as demonstrations of long-lived QD-LED structures are necessary. In this study we consider improvements in QD-LED efficiency.

The original demonstrations of hybrid organic/QD LEDs used QDs blended into hole-transporting polymers, such as poly(phenylvinylene) (PPV),^{1,2} sandwiched between the transparent anode and a metallic cathode. These devices, as well as their extensions that used thick QD multilayers on top of hole-transporting polymers,^{3,4} had low EQEs <0.1%.

A more recent generation of QD-LEDs uses thin (20–60 nm thick) organic charge transporting layers akin to those of OLEDs with layers of QD lumophores embedded between them.^{5–10}

While EQEs for QD-LEDs reported in literature do not exceed 2.1%,^{8,10} ultimately EQEs of these devices are limited by the photoluminescence (PL) efficiency (or quantum yield, QY) of QDs in a thin film, which can be as high as 10%.¹⁴ With higher QD thin film PL efficiencies, EQEs should proportionately increase. Consequently, in this work we employ materials optimized to produce QDs with the highest available PL QY in each part of the visible spectrum. For deep red emission we chose CdZnSe alloyed QD cores passivated with oleic acid, synthesized in a procedure similar to that used by Zhong et al.¹⁵ with PL peak at wavelength $\lambda = 647$ nm in chloroform solution and QY of 50%; for orange emission we chose CdSe/ZnS core–shell QDs passivated with trioctylphosphine (TOP) and trioctylphosphine oxide (TOPO), prepared via well-established procedures,^{16,17} with PL peak at $\lambda = 600$ nm in chloroform and QY of 75%; for green emission we used ZnSe/CdSe/ZnS core-double-shell QDs passivated with hexylphosphonic acid and TOPO synthesized via procedures similar to those used by Ivanov et al.¹⁸ and Steckel et al.¹¹ with PL peak in chloroform at $\lambda = 540$ nm and QY of 65%; for blue emission we chose ZnCdS alloyed QD cores passivated with oleylamine and

[†] These authors equally contributed to the presented work.

[‡] Laboratory of Organic Optics and Electronics, Department of Electrical Engineering and Computer Science.

[§] Department of Chemistry.

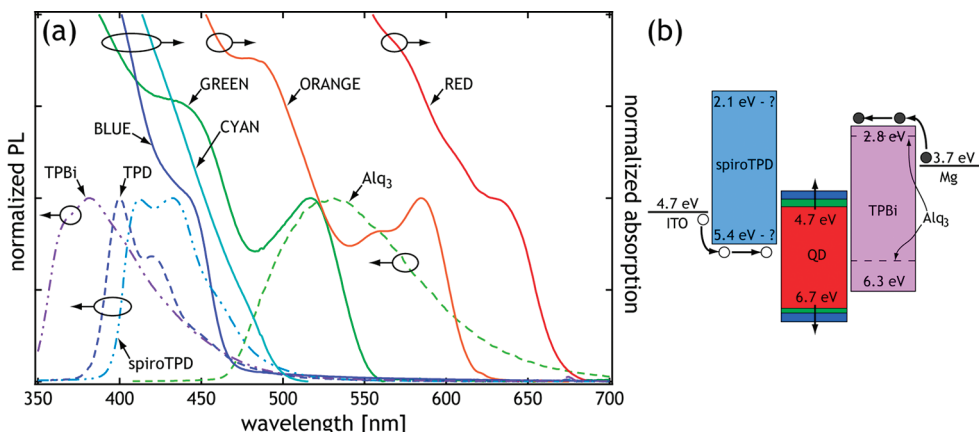


Figure 1. (a) Absorption spectra of red, orange, green, cyan, and blue QDs in chloroform solutions are represented with solid lines. Thin film photoluminescence (PL) spectra of TPD, Alq₃, spiroTPD, and TPBi are shown on the same graph with dashed lines. Organic thin films are prepared via evaporative deposition. Thin film PL is excited by a 337 nm nitrogen laser. (b) Suggested energy band diagram for our QD-LEDs shown relative to ITO and Mg work functions. Arrows indicate the change in position of conduction and valence bands for QDs emitting from red to blue parts of the visible spectrum. The positions of HOMO and LUMO levels of Alq₃, TPD, and TPBi can be found in refs 5 and 7. The positions of QD conduction and valence bands are derived according to Efros and Rosen.²⁶ We use structural similarity of spiroTPD and TPD as well as spiroTPD absorption data available from ref 25 to propose the possible positions of the HOMO and LUMO levels of spiroTPD, since according to our best knowledge they have not been measured (or calculated) yet.

oleic acid produced in a synthetic route similar to that used by Zhong et al.¹⁹ with PL peak at $\lambda = 460$ nm in chloroform and QY of 50%; finally we developed cyan emitters with record solution PL QY of 80% in chloroform by overcoating ZnCdS cores emitting at $\lambda = 490$ nm with ZnS shell. All the synthetic procedures used or developed in this work are described in detail in the Supporting Information.

The second crucial step in QD-LED design is the choice of organic charge transporting layers that surround the QD luminescent centers. In an archetypical QD-LED structure electrons are injected from a metallic cathode into an electron-transporting layer (ETL), holes are injected from a transparent anode into a hole-transporting layer (HTL); carriers then travel toward the layer of QDs. The spectrally narrow electroluminescence (EL) of QD-LEDs is dominated by QD emission, indicating that a majority of the excitons generated in these structures recombine on QD sites. There are two main processes that contribute to the QD EL in QD-LEDs:²⁰ (1) direct carrier injection into QDs followed by exciton formation and recombination resulting in saturated QD emission; (2) exciton formation in organic films followed by nonradiative resonant exciton energy transfer to QDs²¹ yielding QD emission. In addition, there are two main processes limiting QD-LED efficiency: (1) QD charging²⁰ and consequent nonradiative Auger recombination,²² during which an exciton recombines to donate its energy to an unpaired carrier, which then relaxes to the ground state via interactions with phonons; (2) field-induced Onsager exciton dissociation.^{23,24}

Considering the energy alignment of the ground and excited electronic states of QD monolayers and the surrounding organic thin films in a QD-LED can provide insights into the operation of these devices. We note that for organic wide band gap hole-transporting materials used in OLEDs to date the HOMO level is typically positioned between 5.0 and 6.0 eV below the vacuum level.²⁵ As the

same hole-transporting materials are utilized in hybrid QD-LEDs, there is a significant potential energy step for the hole injection into the QD valence band positioned >6.0 eV below the vacuum level.²⁶ The LUMO bands of organic electron-transporting materials are usually found between 2.0 and 3.5 eV below the vacuum level²⁵ and, consequently, there is no potential barrier for electron injection into the QD conduction bands that are between 4.0 and 4.8 eV below the vacuum level.²⁶ The only obstacle for electron injection (which is also a barrier for hole injection) into QDs is the insulating layer of organic ligands that are passivating the QD surface. As the ligand layer is typically ≤ 0.5 nm thick, it forms a minimal tunneling barrier for the carriers that pass through it.

The difference in potential barriers for hole and electron injection into QDs results in carrier imbalance at QD sites and formation of electron–exciton pairs that recombine via the Auger mechanism. As organic hole-transporting materials with low HOMO level are not readily available, we can improve QD-LED performance by enhancing energy transfer from organic films to QDs.²⁰ This route requires finding materials that (1) can efficiently transfer excitons to QDs via Förster mechanism²¹ and (2) do not accept excitons formed on QD sites.

Figure 1a shows absorption spectra of all the QD types (from red to blue) used in our study as well as PL spectra of *N,N'*-bis(3-methylphenyl)-*N,N'*-bis(phenyl)benzidine (TPD) and tris(8-hydroxyquinoline) aluminum (Alq₃), thin films of which are often used in QD-LED fabrication as hole- and electron-transport layers, respectively. It is evident from the spectral overlap between Alq₃ emission and red and orange QD absorption that excitons formed on Alq₃ can efficiently transfer to red and orange QDs.²⁰ In contrast, the absorption spectra of green, cyan, and blue QDs poorly overlap (or do not overlap) with Alq₃ emission spectrum, reducing the rate of energy transfer of Alq₃ excitons to these QDs. Further-

more, spectral overlap indicates that Alq₃ can accept excitons from blue QDs, acting as an exciton sink rather than a source (see Supporting Information for details), hence, limiting the utility of Alq₃ films to only red and orange QD-LEDs. In order to fabricate green and blue QD-LEDs, previous reports utilized either wide band gap hole-blocking layers^{9,11,12} (HBLs) such as 3,4,5-triphenyl-1,2,4-triazole TAZ or thick (up to seven monolayers) QD films¹⁰ to move the exciton formation region away from the Alq₃ interface and minimize the otherwise large Alq₃ emission contribution to QD-LED EL.²⁷

For device structures presented in this study we replace Alq₃ electron transport layer (ETL) with 2,2',2''-(1,3,5-benzenetriyl)-tris(1-phenyl-1-H-benzimidazole) (TPBi), which was previously reported to improve the performance of red QD-LEDs utilizing CdSe/ZnS QDs as emitters.^{7,8} From the spectral overlap between TPBi PL and QD absorption, in Figure 1, it is apparent that exciton energy transfer from TPBi molecules to all the QD types is favorable, with no back transfer expected. Therefore, with TPBi ETL we do not need to use HBLs or thick QD films to achieve narrow QD-LED EL spectra dominated by QD emission.

The commonly used TPD hole transport layer (HTL) has a favorable spectral overlap with QD absorption spectra, indicating that TPD could transfer its excitons to all QD types, with energy transfer to blue QDs expected to be the least efficient process. However, TPD is prone to crystallization upon exposure to oxygen and moisture, which results in poor film morphology that degenerates device performance. To improve the shelf life of our devices, we replace TPD with spiro-*N,N'*-diphenyl-*N,N'*-bis(3-methylphenyl)-(1,1'-biphenyl)-4,4'-diamine (spiroTPD), as its larger (non-flat) molecules are less likely to realign into a polycrystalline structure, and hence film morphology is less likely to change during the device operation. (Note, the latter suggestion is supported by the spiroTPD high glass transition temperature 102 °C as compared to TPD glass transition temperature of 65 °C.²⁵) The overlap of the spiroTPD PL spectrum with the absorption spectra of all the QD types makes it a suitable exciton donor during QD-LED operation (Figure 1).

The final important step in QD-LED fabrication is the choice of QD deposition technique. Since all the QDs used in our study are fabricated via different synthetic procedures,^{15–19} and consequently their surfaces are passivated by different organic ligands, it is beneficial to identify a flexible deposition method that allows controlled placement of QD types with different surface chemistries into an identical device structure. We chose to utilize a recently demonstrated QD contact printing technique,²⁸ which allows us to deposit close-packed monolayers of solvent-free QDs onto evaporated spiroTPD HTL, without exposing the device structure to solvents that could precipitate thin film morphological changes.

Figure 2 shows the atomic force microscope (AFM) images of close-packed monolayers of different QD types deposited onto 40 nm thick spiroTPD layer, which was evaporated on top of a thin film of spun-cast hole injecting polymer poly(3,4-ethylenedioxythiophene):poly(styrene-

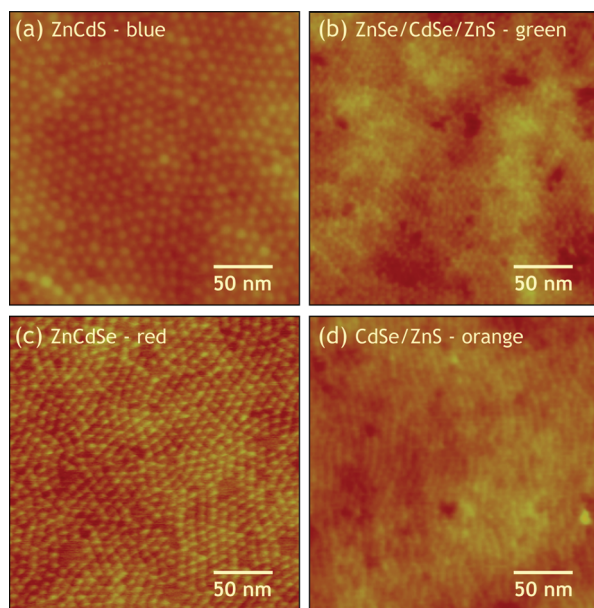


Figure 2. AFM height images show close packed monolayers of different QD types on top of a 40 nm thick spiroTPD film: (a) blue-luminescing CdZnS alloyed cores passivated with oleylamine and hexylphosphonic acid, with rms roughness of 0.9 nm; (b) green-luminescing ZnSe/CdSe/ZnS core double-shell QDs passivated with oleic acid and TOP, with rms roughness of 0.5 nm; (c) red-luminescing ZnCdSe alloyed cores passivated with oleic acid, with rms roughness of 0.4 nm; (d) orange-luminescing CdSe/ZnS core–shell QDs passivated with TOPO/TOP, with rms roughness of 0.7 nm. (1 μm² AFM images of QD monolayers are available in Supporting Information. The long-range quality of contact printed QD monolayers is addressed in detail ref 29.)

sulfonate) (PEDOT:PSS) that coats the indium tin oxide (ITO) anode. All AFM images in Figure 3 show film rms roughness of ≤1 nm, indicating the quality of the print-deposition process, which relies on compatibility of all the QD types with spiroTPD surface, as well as with the surface of parylene-C coated poly(dimethylsiloxane) (PDMS) stamps used for contact printing. (Note: in order to distinguish between QD monolayers and multilayers, the thickness of QD films is calibrated based on the grain analysis of AFM images as described in detail in the Supporting Information of ref 28). After QD deposition, the structures shown in Figure 2 are completed by evaporation of 40 nm TPBi film and 100 nm Mg:Ag cathode with 20 nm protective Ag overlayer (please see Supporting Information for device fabrication details). The photograph inset of Figure 2 demonstrates that the print deposition on top of the spiroTPD can be applied multiple times on the same substrate²⁷ to generate three different color QD-LEDs.

Photographs of QD-LED pixels in Figure 3a and the normalized EL spectra in Figure 3b show bright multicolor emission from the red, orange, green, cyan, and blue QD-LEDs fabricated using the 40 nm thick spiroTPD HTL and TPBi ETL and printed close-packed monolayers of QD types described above. While red, orange, green, and cyan QD-LEDs exhibit narrow EL spectra solely due to QD emission, blue QD-LEDs show minor organic EL contribution, due to incomplete transfer of excitons formed on spiroTPD and TPBi molecules (see Supporting Information for details.)

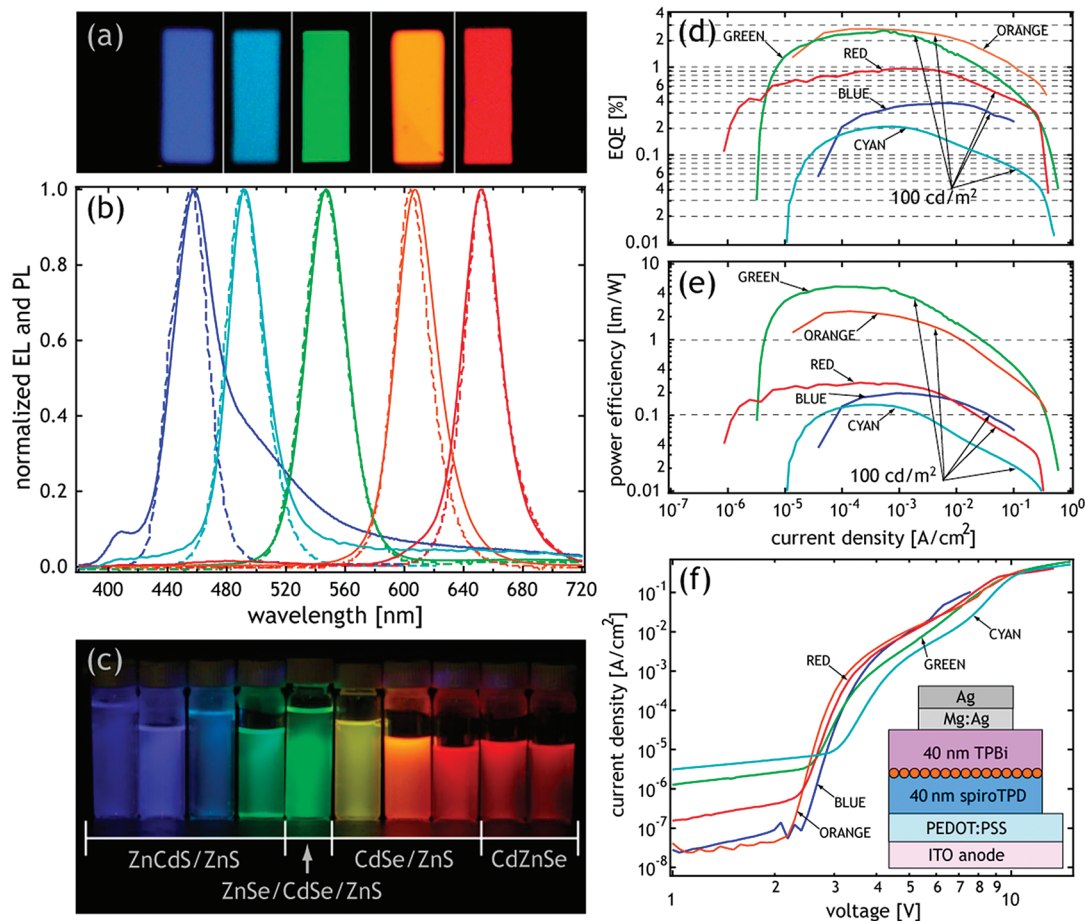


Figure 3. (a) Composite of photographs of $0.6 \times 1.9 \text{ mm}^2$ QD-LED pixels operating at applied bias voltage of 6 V for blue and cyan, 4 V for green and orange, and 5 V for red. (b) Electroluminescence spectra (solid lines) of QD-LEDs from (a) at applied bias voltages of 5 V for blue, green, and orange, 6 V for cyan, and 4 V for red. Photoluminescence spectra (dashed lines) have been measured in QD monolayers for the red (excited with 532 nm laser), orange, and green (excited with 408 nm laser) QDs and in hexane solutions for the blue and cyan QDs (excitation with 350 nm light from a xenon lamp) due to lack of absorption of the blue and cyan QD monolayers at wavelengths >350 nm. (c) Photograph of the photoluminescence of chloroform solutions of different QD types used in this study. In this photograph, QD solutions are excited by a UV lamp with emission centered at a wavelength of 365 nm. (d) External quantum efficiency in % and (e) power efficiency in lm/W for red, orange, green, cyan, and blue QD-LEDs are plotted vs current density. (f) Current–voltage characteristics of the different color QD-LEDs. Inset shows the schematic cross section of the device structure used in this study.

Even with the minor organic EL contribution, QD-LED pixels based on blue ZnCdS QDs appear blue to the eye. The photograph in Figure 3c shows the chloroform solutions of the QDs used in the current study as well as other QD colors obtained from the same material sets that can be used in QD-LED fabrication. The materials exemplify the high PL QY obtained through the synthetic methods described above and detailed in the Supporting Information.

External quantum efficiencies (EQEs) of our QD-LEDs are plotted in Figure 3d as a function of the injected current density, with the 100 cd/m^2 luminance operating point indicated in the plot. The peak EQE values are 1% for red, 2.7% for orange, 2.6% for green, 0.2% for cyan, and 0.4% for blue QD-LEDs. The corresponding peak values of power efficiency (Figure 3e) are 0.25 lm/W for red, 2.4 lm/W for orange, 5 lm/W for green, 0.1 lm/W for cyan, 0.2 lm/W for blue QD-LEDs (Table 1). To our knowledge, EQE and power efficiency values for orange, green, and blue QD-LEDs represent record values reported to date for hybrid organic-QD LEDs.

Table 1

QD-LED color	peak EQE (%)	brightness at peak EQE (cd/m^2)	EQE at 100 cd/m^2 (cd/m^2)
blue (EL _{max} at 460 nm)	0.4	15	0.3
cyan (EL _{max} at 490 nm)	0.2	3	0.05
green (EL _{max} at 545 nm)	2.6	28	2.2
orange (EL _{max} at 600 nm)	2.7	13	2.3
red (EL _{max} at 650 nm)	1.0	7	0.5

While EQE of our green QD-LEDs is >4 times higher than previously reported values, we observe only a slight increase in blue QD-LED EQE. This result is consistent with our previous observations, where we find that the QD EL in QD-LEDs is primarily due to the excitons that have been nonradiatively transferred to QDs from organic materials.²⁰ In previous QD-LED designs green QD-LEDs could only operate via direct charge injection and energy transfer from TPD (or polymer TPD derivatives) HTL.^{9–11} In these earlier demonstrations exciton formation in organic HTL is inhibited by electron accumulation in neighboring QD sites. In addition, the exciton formation in Alq₃ ETL was purposely eliminated by a HBL to avoid Alq₃ contribution to QD-LED

EL spectra. Consequently, the EQEs of previously reported green QD-LEDs did not exceed 0.5–0.6%.^{9–11} In our design we eliminate HBL and allow exciton formation in TPBi ETL that can transfer its exciton energy to green QDs. The operation of blue QD-LEDs is still limited by inefficient and incomplete energy transfer from organics, due to the weak absorption of blue QDs across the spiroTPD and TPBi emission spectra. The direct charge injection may have higher proportional contribution to the blue QD-LED electroluminescence, which is manifested in its low EQE value of 0.4%. Both energy transfer and charge injection into cyan ZnCdS/ZnS core–shell QDs are further inhibited by a thick (~2 nm) wide band gap ZnS shell, and consequently the EQE of cyan QD-LEDs is 2 times lower than that of blue QD-LEDs, despite the increased solution PL QY of overcoated QDs.

Our work demonstrates that through the choice of high QY colloidal QDs and selection of wide-band-gap charge transport layers, the EQE of hybrid organic/QD LEDs can be increased. While we can routinely obtain EQEs between 1% and 2.5% for QD-LEDs emitting in green and red parts of the visible spectrum, achieving high EQE blue QD-LEDs remains a challenge that might be remedied by design and synthesis of wide band gap hole- and electron-transporting organic materials for improved exciton energy transfer and direct charge injection into blue QDs.

Acknowledgment. This work was supported in part by the NSF-MRSEC Program (DMR-0213282), making use of its Shared Experimental Facilities, and the U.S. Army through the Institute for Soldier Nanotechnologies (DAAD-19-02-0002) and NIRT (subcontract GLV13-01). We would like to thank Professor I. Kymmissis of Columbia University for valuable discussions.

Supporting Information Available: Details of synthesis, device fabrication and testing, overlap between blue ZnCdS QD emission and Alq₃ absorption, and spiroTPD/TPBi OLED photoluminescence and electroluminescence spectra and AFM images of QD monolayers. This material is available free of charge via the Internet at <http://pubs.acs.org>.

References

- (1) Colvin, V. L.; Schlamp, M. C.; Alivisatos, A. P. *Nature* **1994**, *370*, 354–357.
- (2) Dabbousi, B. O.; Bawendi, M. G.; Onitsuka, O.; Rubner, E. M. F. *Appl. Phys. Lett.* **1995**, *66*, 1316–1318.
- (3) Schlamp, M.; Peng, X.; Alivisatos, A. P. *J. Appl. Phys.* **1997**, *82*, 5837.
- (4) Mattoussi, H.; Radzilowski, L. H.; Dabbousi, B. O.; Fogg, D. E.; Schrock, R. R.; Thomas, E. L.; Bawendi, M. G.; Rubner, M. F. *J. Appl. Phys.* **1998**, *83*, 7965–7975.
- (5) Coe, S.; Woo, W. K.; Bawendi, M.; Bulovic, V. *Nature* **2002**, *420*, 800–803.
- (6) Coe-Sullivan, S.; Steckel, J. S.; Woo, W.-K.; Bawendi, M.; Bulovic, V. *Adv. Funct. Mater.* **2005**, *15*, 1117–1124.
- (7) Zhao, J.; Bardecker, J. A.; Munro, A. M.; Liu, M. S.; Niu, Y.; Ding, I.-K.; Luo, J.; Chen, B.; Jen, A. K.-Y.; Ginger, D. S. *Nano Lett.* **2006**, *6*, 463–467.
- (8) Niu, Y.-H.; Munro, A. M.; Cheng, Y.-J.; Tian, Y.; Liu, M. S.; Zhao, J.; Bardecker, J. A.; Jen-La Plante, I.; Ginger, D. S.; Jen, A. K.-Y. *Adv. Mater.* **2007**, *19*, 3371–3376.
- (9) Anikeeva, P. O.; Halpert, J. E.; Bawendi, M. G.; Bulovic, V. *Nano Lett.* **2007**, *7*, 2196.
- (10) Sun, Q.; Wang, Y. A.; Li, L. S.; Wang, D.; Zhu, T.; Xu, J.; Yang, C.; Li, Y. *Nat. Photonics* **2007**, *1*, 717–722.
- (11) Steckel, J. S.; Snee, P. T.; Coe-Sullivan, S.; Zimmer, J. P.; Halpert, J. E.; Anikeeva, P. O.; Kim, L.; Bulovic, V.; Bawendi, M. G. *Angew. Chem., Int. Ed.* **2006**, *45*, 5796–5799.
- (12) Steckel, J.; Zimmer, J.; Coe-Sullivan, S.; Stott, N.; Bulovic, V.; Bawendi, M. *Angew. Chem., Int. Ed.* **2004**, *43*, 2154.
- (13) Adachi, C.; Baldo, M.; Thompson, M. E.; Forrest, S. R. *J. Appl. Phys.* **2001**, *90*, 5048.
- (14) Klimov, V. I.; Mikhailovsky, A. A.; Xu, S.; Malko, A.; Hollingsworth, J. A.; Leatherdale, C. A.; Eisler, H.-J.; Bawendi, M. G. *Science* **2000**, *290*, 314–317.
- (15) Zhong, X.; Han, M.; Dong, Z.; White, T. J.; Knoll, W. *J. Am. Chem. Soc.* **2003**, *125*, 8589–8594.
- (16) Hines, M. A.; Guyot-Sionnest, P. *J. Phys. Chem.* **1996**, *100*, 468.
- (17) Dabbousi, B. O. et al. *J. Phys. Chem. B* **1997**, *101*, 9463–9475.
- (18) Ivanov, S. A.; Nanda, J.; Piryatinski, A.; Achermann, M.; Balet, L. P.; Bezel, I. V.; Anikeeva, P. O.; Tretiak, S.; Klimov, V. *J. Phys. Chem.* **2004**, *108*, 10625.
- (19) Zhong, X.; Feng, Y.; Knoll, W.; Han, M. *J. Am. Chem. Soc.* **2003**, *125*, 13559–13563.
- (20) Anikeeva, P. O.; Madigan, C. F.; Halpert, J. E.; Bawendi, M. G.; Bulović, V. *Phys. Rev. B* **2008**, *78*, 085434 1–8.
- (21) Förster, Th. *Ann. Phys.* **1948**, *6*, 55.
- (22) Klimov, V. I.; Mikhailovsky, A. A.; McBranch, D. W.; Leatherdale, C. A.; Bawendi, M. G. *Science* **2000**, *287*, 1011.
- (23) Onsager, L. *Phys. Rev.* **1938**, *15*, 554.
- (24) Huang, H.; Dorn, A.; Nair, G.; Bulović, V.; Bawendi, M. G. *Nano Lett.* **2007**, *7*, 3781.
- (25) Luminescence Technology Corp., <http://www.lumtec.com.tw>.
- (26) Al. L., Efros; Rosen, M. *Annu. Rev. Mater. Sci.* **2000**, *30*, 475.
- (27) Coe-Sullivan, S.; Woo, W. K.; Steckel, J. S.; Bawendi, M.; Bulovic, V. *Org. Electron.* **2003**, *4*, 123–130.
- (28) Kim, L.; Anikeeva, P. O.; Coe-Sullivan, S.; Steckel, J. S.; Bawendi, M. G.; Bulović, V. *Nano Lett.* **2008**, *8*, 4513–4517.
- (29) Kim, L. MEng Thesis, Department of Electrical Engineering and Computer Science, MIT, 2006.

NL9002969